Inorg. Chem. **2002**, *41*, 3128–3136

Enhancing Reactivity via Structural Distortion

Dirk Schweitzer, Jason Shearer, Durrell K. Rittenberg, Steven C. Shoner, Jeffrey J. Ellison, Reza Loloee, Scott Lovell, David Barnhart, and Julie A. Kovacs*

Department of Chemistry, University of Washington, Seattle, Washington 98195

Received August 20, 2001

To examine how small structural changes influence the reactivity and magnetic properties of biologically relevant metal complexes, the reactivity and magnetic properties of two structurally related five-coordinate Fe(III) thiolate compounds are compared. (Et,Pr)-ligated [Fe(III)($S_2^{Me2}N_3$(Et,Pr))]PF_6 (**3**) is synthesized via the abstraction of a sulfur from alkyl persulfide ligated [Fe(III)($S_2^{Me2}N_3$(Et,Pr))-S^{pers}]PF_6 (**2**) using PEt_3. (Et,Pr)-**3** is structurally related to (Pr,Pr)-ligated [Fe(III)($S_2^{Me2}N_3$(Pr,Pr))]PF_6 (**1**), a nitrile hydratase model compound previously reported by our group, except it contains one fewer methylene unit in its ligand backbone. Removal of this methylene distorts the geometry, opens a S–Fe–N angle by ∼10°, alters the magnetic properties by stabilizing the $S = 1/2$ state relative to the $S = 3/2$ state, and increases reactivity. Reactivity differences between **3** and **1** were assessed by comparing the thermodynamics and kinetics of azide binding. Azide binds reversibly to both (Et,Pr)-**3** and (Pr,Pr)-**1** in MeOH solutions. The ambient temperature K_{eq} describing the equilibrium between five-coordinate **1** or **3** and azide-bound **1-N$_3$** or **3-N$_3$** in MeOH is ∼10 times larger for the (Et,Pr) system. In CH_2Cl_2, azide binds ∼3 times faster to **3** relative to **1**, and in MeOH, azide dissociates 1 order of magnitude slower from **3-N$_3$** relative to **1-N$_3$**. The increased on rates are most likely a consequence of the decreased structural rearrangement required to convert **3** to an approximately octahedral structure, or they reflect differences in the LUMO (vs SOMO) orbital population (i.e., spin-state differences). Dissociation rates from both **3-N$_3$** and **1-N$_3$** are much faster than one would expect for low-spin Fe^{III}. Most likely this is due to the labilizing effect of the thiolate sulfur that is trans to azide in these structures.

Introduction

Enzymes catalyze reactions by holding a reactant in a near transition state. Proteins play a critical role in this by, for example, constraining geometries and/or providing a reaction cavity that contains appropriately charged or H-bonding residues, positioned so as to stabilize a specific structure. With metalloenzymes, this more reactive state is referred to as an entatic[1,2] or rack state.[3,4] The classic example of a metalloenyzme in an entatic state is blue copper proteins. With blue copper proteins electron transfer rates are enhanced as a consequence of protein constraints that hold the Cu(II) metal ion in a highly distorted geometry.[5] The thermodynamics of reduction also become more favorable as a consequence of these constraints. With metalloenzymes involved in binding and activating substrates, it is possible that the protein increases reactivity by constraining angles so as to make a metal ion more reactive. However, deviations from idealized geometries (i.e., angle distortions) generally result in structures which are less stable, and therefore more difficult to isolate outside of a protein environment. Ligands capable of imposing constrained geometries require careful design, aided by three-dimensional structure programs (e.g., SPARTAN), and require multistep syntheses, involving protection and deprotection of sulfur when thiolates are incorporated.

Examples of synthetic systems that display enhanced reactivity as a consequence of ligand constraints include Stack's peralkylated diamine ligated binuclear copper complex, which cleaves the O−O bond of dioxygen.[6] Stack has also shown that subtle structural changes involving the incorporation of a methoxy substituent into a tris(2-pyridyl)-

* E-mail: kovacs@chem.washington.edu.

(1) Vallee, B. L.; Williams, R. J. P. *Proc. Natl. Acad. Sci. U.S.A.* **1968**, *59*, 498−505.
(2) Williams, R. J. P. *Eur. J. Biochem.* **1995**, *234*, 363−381.
(3) Lumry, R.; Eyring, H. *J. Phys. Chem.* **1954**, *58*, 110−120.
(4) Malmström, B. G. *Eur. J. Biochem.* **1994**, *223*, 711−718.
(5) Solomon, E. I.; LaCroix, L. B.; Randall, D. W. *Pure Appl. Chem.* **1998**, *70*, 799−808.
(6) Mahadevan, V.; Henson, M. J.; Solomon, E. I.; Stack, T. D. P. *J. Am. Chem. Soc.* **2000**, *122*, 10249.

10.1021/ic0109187 CCC: $22.00
Published on Web 05/24/2002

carbinol ligated Cu complex dramatically alters ligand exchange behavior.[7] Lippard and Karlin have shown that steric constraints control the reactivity of Fe(II) complexes with CO.[8] Busch has shown that the propensity for transition-metal macrocyclic complexes to bind additional ligands is dramatically altered by changing the size of the macrocycle.[9] And finally, Borovik recently demonstrated that when bulky groups containing H-bonding donors are incorporated into an encapsulating ligand, stable Fe^{III}−OH and Fe−oxo species can be isolated.[10]

The coordinatively unsaturated Fe(III) complex [Fe(III)-($S_2^{Me2}N_3$(Pr,Pr))]PF_6 (**1**) was synthesized as a model for the

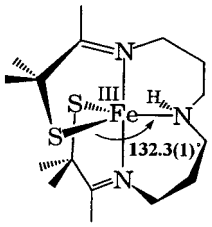

1

metalloenzyme nitrile hydratase (NHase)[11] and was shown to possess an open angle ($S-Fe-N_{amine}$ = 132.3(1)°) as a consequence of ligand constraints.[12] The ligand backbone of **1** (referred to as (Pr,Pr)) is derived from *N*-(3-aminopropyl)-1,3-propanediamine. Nitric oxide[13] and azide[12] bind to the open angle of **1** to afford models for both the NO-inactivated[14,15] and azide-inhibited[16] forms of NHase, respectively. Compound **1** does not readily bind nitriles, the substrate of NHase, at ambient temperatures, however. In an attempt to increase reactivity, a methylene unit was removed from the (Pr,Pr) ligand backbone of **1**. It was reasoned that a shorter ligand would be incapable of supporting the idealized 120° angles expected for a trigonal bipyramid, resulting in an even more distorted structure. Herein, we describe the influence that this small perturbation to ligand structure has on the structural, magnetic, and reactivity properties of a thiolate/imine chelated Fe(III) complex.

Experimental Section

General Methods. All manipulations were performed using Schlenk line techniques or in a glovebox under an atmosphere of N_2. Reagents and solvents were purchased from commercial suppliers. MeOH (Na) and MeCN (CaH_2) were dried and distilled before use. Infrared spectra were recorded as KBr pellets on a Perkin-Elmer 1600 FTIR spectrometer. NMR spectra were recorded on an AF300 spectrometer at ambient temperature. ^{31}P NMR shifts are cited relative to 85% H_3PO_4. UV/vis−near-IR spectra were recorded on a Hewlett-Packard 8450 diode array spectrophotometer. Cyclic voltammetry experiments were performed using a PAR 273 potentiostat with a glassy carbon working electrode, a platinum wire counter electrode, an SCE reference electrode, and a 0.1 M solution of $[CH_3(CH_2)_3]_4N(PF_6)$ supporting electrolyte in MeCN. The ferrocene$^{+/0}$ couple was +400 mV under these conditions. Magnetic susceptibility measurements in the solid state (polycrystalline sample) were performed using a Quantum Design MPMS SQUID susceptometer (H = 1000 G) at Michigan State University. Solution magnetic moments were determined on an AF300 NMR spectrometer using the Evans method, as modified for superconducting solenoids.[17] Van Geet's method was used to determine the temperature of the measurement.[18] Diamagnetic corrections were taken from the literature.[19] EPR spectra were recorded on an EPX Bruker using the following glasses and temperatures: **1**: CH_2Cl_2/toluene (1/1), 125 K; **3**: CH_2Cl_2/toluene (1/1), 150 K; **1-N$_3$** and **3-N$_3$**: CH_2Cl_2/toluene (1/1), 130 K; **2**: MeOH/EtOH (9/1), 141 K. The following parameters were utilized: microwave frequency = 9.395 GHz for **1**, 9.380 GHz for **1-N$_3$**, 9.404 GHz for **2**, 9.390 GHz for **3**, 9.375 GHz for **3-N$_3$**; microwave power = 6.331 mW for **1**, **1-N$_3$**, and **3**, 12.631 mW for **2**, 0.633 mW for **3-N$_3$**; modulation amplitude = 5.00 G for **1**, **1-N$_3$**, **3**, and **3-N$_3$**, 3.00 G for **2**; modulation frequency = 10.00 kHz for **1**, **1-N$_3$**, **3**, and **3-N$_3$**, 100.00 kHz for **2**; receiver gain = 1.59×10^5 for **1** and **3**, 1.26×10^5 for **1-N$_3$** and **3-N$_3$**, 1.00×10^5 for **2**. Elemental analyses were performed by Atlantic Microlab, Norcross, GA.

Preparation of Compounds. Synthesis of [Fe(III)($S_2^{Me2}N_3$-(Et,Pr))-S^{pers}]PF_6 (2) from (A) $FeCl_2$. A MeOH solution (30 mL) of NaOH (800 mg, 20 mmol) and 3-mercapto-3-methyl-2-butanone[20] (2.364 g, 20 mmol) was added dropwise to a MeOH solution (40 mL) of $FeCl_2$ (1.266 g, 10 mmol). After 15 min, *N*-(2-aminoethyl)-1,3-propanediamine (1.172 g, 10 mmol) was added. The mixture was stirred for 5 h, at which time $FeCp_2PF_6$ (3.476 g, 10.5 mmol) was added. After stirring for ∼60 h, the mixture was evaporated to dryness under vacuum. Recrystallization from MeCN/Et_2O (10:1) afforded 0.990 g (1.8 mmol) of crystalline **2**. Electronic absorption spectrum in MeOH, λ_{max}, nm (ϵ, M^{-1} cm^{-1}): 211 (15 500), 300 (9400), 553 (1950). Elemental analysis calculated for $C_{15}H_{29}N_3F_6FePS_3$: C, 32.85; H, 5.33; N, 7.66. Found: C, 32.91; H, 5.13; N, 7.62. Reduction potential: E(irreversible) = −790 mV (vs SCE). Magnetic moment: 2.02 μ_B (301 K, MeCN solution) and 2.15 μ_B (300 K, solid state). X-band EPR (141 K): g = 2.17, 2.11, 1.99.

Synthesis of [Fe(III)($S_2^{Me2}N_3$(Et,Pr))-S^{pers}]PF_6 (2) from (B) $FeCl_3$. A MeOH solution (30 mL) of NaOH (800 mg, 20 mmol) and 3-mercapto-3-methyl-2-butanone[20] (2.364 g, 20 mmol) was added dropwise to a MeOH solution (40 mL) of $FeCl_3$ (1.622 g, 10 mmol). *N*-(2-aminoethyl)-1,3-propanediamine (1.172 g, 10 mmol) was added after 15 min of stirring. Thereafter, KPF_6 (2.1 g, 11.4 mmol) was added. After the mixture was stirred for ∼90 h, it was evaporated to dryness under vacuum and worked up as described in method A ($FeCl_2$). Yield: 0.680 g (1.24 mmol). This material is spectroscopically identical to the product of reaction A.

(7) Jonas, R. T.; Stack, T. D. P. *Inorg. Chem.* **1998**, *37*, 6615.
(8) Karlin, K. D.; Lippard, S. J. *J. Am. Chem. Soc.* **1976**, *98*, 6951.
(9) Busch, D. H. *Chem. Rev.* **1993**, *93*, 847
(10) MacBeth, C. E.; Golombek, A. P.; Young, V. G., Jr.; Yang, C.; Kuczera, K.; Hendrich, M. P.; Borovik, A. S *Science* **2000**, *289*, 938−941.
(11) Endo, I.; Odaka, M. *J. Mol. Catal. B: Enzymatic* **2000**, *10*, 81−86 and references therein.
(12) Ellison, J. J.; Nienstedt, A.; Shoner, S. C.; Barnhart, D.; Cowen, J. A.; Kovacs, J. A. *J. Am. Chem. Soc.* **1998**, *120*, 5691−5700.
(13) Schweitzer, D.; Ellison, J. J.; Shoner, S. C.; Lovell, S.; Kovacs, J. A. *J. Am. Chem. Soc.* **1998**, *120*, 10996−10997.
(14) Odaka, M.; Fujii, K.; Hoshino, M.; Noguchi, T.; Tsujimura, M.; Nagashima, S.; Yohada, N.; Nagamune, T.; Inoue, I.; Endo, I. *J. Am. Chem. Soc.* **1997**, *119*, 3785−3791.
(15) Nagashima, S. N., M.; Naoshi, D.; Tsujimura, M.; Takio, K.; Odaka, M.; Yohda, M.; Kamiya, N.; Endo, I. *Nat. Struct. Biol.* **1998**, *5*, 347−351.
(16) Sugiura, Y.; Kuwahara, J.; Nagasawa, T.; Yamada, H. *J. Am. Chem. Soc.* **1987**, *109*, 5848−50.
(17) Schubert, E. M. *J. Chem. Educ.* **1992**, *69*, 62.
(18) Van Geet, A. L. *Anal. Chem.* **1968**, *40*, 2227−2229.
(19) Mulay, L. N.; Boudreaux, E. A. *Theory and Applications of Molecular Diamagnetism*; John Wiley & Sons: New York, 1976.
(20) Asinger, F.; Thiel, M.; Esser, G. *Liebigs Ann. Chem.* **1957**, *610*, 33−49.

Synthesis of [Fe(III)($S_2^{Me2}N_3$(Et,Pr))]PF_6 (3). Four equivalents of PEt_3 (8.0 mmol, 8 mL of a 1.0 M solution in THF) were added to a solution of **2** (1.1 g, 2.0 mmol) in MeCN (25 mL). After the mixture was stirred for 24 h, it was evaporated to dryness under vacuum. The residue was extracted with Et_2O to remove $SPEt_3$. The resulting residue was then dissolved in CH_2Cl_2 and filtered. Crystals of **3** were grown by slow diffusion of Et_2O into this CH_2Cl_2 solution at ambient temperature. Yield: 0.730 g (1.4 mmol, 70%). Electronic absorption spectrum in MeOH, λ_{max}, nm (ϵ, M^{-1} cm^{-1}): 207 (15 400), 316 (7300), 494 (1530), 532 (1520). Elemental analysis calculated for $C_{15}H_{29}N_3F_6FePS_2$: C, 34.89; H, 5.66; N, 8.14. Found: C, 34.72; H, 5.50; N, 8.00. Reduction potential: $E_{1/2}$(reversible) = −455 mV (vs SCE). Magnetic moment: 2.19 μ_B (301 K, MeCN solution) and 2.07 μ_B (300 K, solid state). EPR (150 K): g = 2.12, 2.07, 2.02.

Synthesis of [Fe(III)($S_2^{Me2}N_3$(Et,Pr))(N_3)] (3-N_3). A MeCN solution (25 mL) containing **3** (506 mg, 0.98 mmol) and $N(Me)_4N_3$ (179 mg, 1.54 mmol) was stirred for 30 min. The mixture was then filtered through Celite. The resulting mixture was then evaporated to dryness, and the residue was extracted with THF (20 mL). The THF solution was then filtered and layered with Et_2O (105 mL). After standing for 4 days at − 35 °C, a black crystalline solid had formed. Yield: 0.150 g (0.36 mmol, 37%). Electronic absorption spectrum in CH_2Cl_2, λ_{max}, nm (ϵ, M^{-1} cm^{-1}): 243 (12 900), 285 (9750), 335 (7050), 474 (1570), 762 (970). Elemental analysis calculated for $C_{15}H_{29}N_6FeS_2$: C, 43.58; H, 7.07; N, 20.33. Found: C, 43.68; H, 7.23; N, 17.92. Reduction potential: E(irreversible) = −590 mV (vs SCE). Magnetic moment: 2.16 μ_B (300 K, MeCN solution) and 2.26 μ_B (300 K, solid state). IR (KBr): $\nu_a(N_3^-)$ = 2031 cm^{-1}. EPR (130 K): g = 2.19, 2.16, 1.98.

Azide Binding Studies. Azide binding studies were performed using freshly prepared solutions of **3** (1 mM) and tetra(*n*-butyl)-ammonium azide in MeOH. Solutions were maintained at a constant ionic strength (I = 0.06 M) using an appropriate amount of tetra-(*n*-butyl)ammonium nitrate. All concentrations were corrected then for changes in the density of MeOH upon cooling as previously described.[21] After mixing, solutions containing varying amounts of azide were then transferred into a custom-designed low-temperature quartz optical Dewar. The amount of tetra(*n*-butyl)-ammonium azide was selected such that 20%−80% of the iron complex was azide-bound. This range gave the least amount of error when calculating equilibrium constants. Equilibrium constants were determined at five different temperatures using the appropriate cryogen (ice−water (0 °C), ethylene glycol/CO_2 (−15 °C), CCl_4/CO_2 (−23 °C), and MeCN/CO_2 (−46 °C)). To minimize the error in K_{eq} calculations, absorption spectra were recorded at the wavelength (551 nm) that gave the greatest difference between unbound and bound species, [Fe(III)($S_2^{Me2}N_3$(Et,Pr))]PF_6 (**3**) and [Fe(III)($S_2^{Me2}N_3$(Et,Pr))(N_3)] (**3-N_3**), respectively. The 551 nm extinction coefficient of [Fe(III)($S_2^{Me2}N_3$(Et,Pr))]PF_6 (**3**) at I = 0.06 mol/L was found to be 1590 ± 35 M^{-1} cm^{-1} at 22, 0, and −15 °C. It was 1567 ± 30 M^{-1} cm^{-1} at −23 °C and 1475 ± 45 M^{-1} cm^{-1} at −46 °C. The 551 nm extinction coefficient of [Fe(III)($S_2^{Me2}N_3$-(Et,Pr))(N_3)] (693 ± 25 M^{-1} cm^{-1}) was determined using 60 equiv of tetra(*n*-butyl)ammonium azide, where complete binding is observed at all of the temperatures investigated. Equilibrium constants were calculated using eqs 1 and 2[22] and determined to be K_{eq}(22 °C) = 110 ± 20 M^{-1}, K_{eq}(0 °C) = 210 ± 40 M^{-1}, K_{eq}-(−15 °C) = 470 ± 90 M^{-1}, K_{eq}(−23 °C) = 720 ± 140 M^{-1}, and K_{eq}(−46 °C) = 4950 ± 800 M^{-1}. Thermodynamic parameters ΔH = −7.5 ± 0.6 kcal/mol and ΔS = −16.6 ± 2.5 cal/(mol K) were determined from a van't Hoff plot.

$$[\mathbf{3}\text{-}\mathbf{N_3}] = \frac{A - \epsilon_{\mathbf{3}}[\mathbf{3}]_0}{\epsilon_{\mathbf{3}-\mathbf{N_3}} - \epsilon_{\mathbf{3}}} \quad (1)$$

$$K_{eq} = \frac{[\mathbf{3}\text{-}\mathbf{N_3}]}{([\mathbf{3}]_0 - [\mathbf{3}\text{-}\mathbf{N_3}])([N_3^-]_0 - [\mathbf{3}\text{-}\mathbf{N_3}])} \quad (2)$$

Kinetic Measurements. Kinetic measurements were performed using an OLIS RSA monochromator attached to an OLIS USA stopped-flow mixing device. The rates of azide binding to **1** and **3** were measured in methanol, acetonitrile, or methylene chloride. One milimolar solutions of **1** and **3** were injected into an equal volume of a $^nBu_4NN_3$ (300 mM) solution in the same solvent at ambient temperature. Rate constants (k_{on}) were determined by fitting the kinetic trace to a first-order rate constant. Dissociation rate constants in MeOH were then determined according to

$$k_d = \frac{k_{on}}{K_{eq}} \quad (3)$$

where K_{eq} is the equilibrium binding constant at room temperature.

X-ray Data Collection and Structure Solution and Refinement. X-ray quality crystals of **2**, **3**, **3-N_3**, and [Fe(II)($S_2^{Me2}N_3$-(Et,Pr))] were grown by slow diffusion of Et_2O into an MeCN solution inside a glovebox. Crystals were immersed in Paratone 8277 oil (Exxon), mounted on a glass fiber, and then immediately placed in a low-temperature N_2(g) stream. X-ray data for **2**, **3**, and **3-N_3** were collected at −112 °C using a Nonius Kappa CCD diffractometer (Mo Kα, λ = 0.710 70 Å). The structures were solved by direct methods (SIR 92)[23] and refined with SHELXL97.[24] X-ray data for [Fe(II)($S_2^{Me2}N_3$(Et,Pr))] was collected at −90 °C using an Enraf-Nonius CAD4 diffractometer (Mo Kα, λ = 0.709 30 Å). Data indexing, integration, and scaling for [Fe(II)($S_2^{Me2}N_3$-(Et,Pr))] was carried out using XCAD4 software. The refinement was performed using SHELXL97. Compound **2** was found to be in a noncentrosymmetric space group (*Cc*, No. 9). However, its absolute structure parameter was found to be 0.491(14), indicative of racemic twinning. Compounds **3**, **3-N_3**, and [Fe(II)($S_2^{Me2}N_3$-(Et,Pr))] were found to crystallize in centrosymmetric space groups, containing both enantiomers in a 1:1 ratio. Cationic **3** (Figure 2) was located on a crystallographic 2-fold axis which bisects the S1−Fe−S1′ angle. Amine nitrogen N2 was found to lie 0.51 Å away from this 2-fold axis, and as a result, N2 and the ethyl and propyl carbons (C7, C14, C15) were found to be disordered, with a 50% occupancy factor. Most of the molecule was not affected by this disorder, however. Atoms C1−C6, N1, and S1 were given site occupancies of 1.0. Within the disordered portion of the ligand backbone, the mean C−C (C14−C15 = 1.555(8) Å, C6−C14 = 1.431(7) Å, C6−C7 = 1.634(8) Å) and C−N (N2−C15 = 1.502-(7) Å, N2−C7′ = 1.520(8) Å) distances are typical (within 3σ), indicating that the disorder was modeled appropriately. An ORTEP diagram (Figure S-8), as well as drawings (Figure S-9) that display this disorder are included in the Supporting Information. Relevant crystallographic information is summarized in Table 1. Complete refinement details are given in the Supporting Information.

(21) Sun, T. F.; Schouten, J. A.; Trappeniers, N. J.; Biswas, S. N. *J. Chem. Thermodyn.* **1988**, *20*, 1089−1096.
(22) Drago, R. S. *Physical Methods for Chemists*, 2nd ed.; Saunders College Publishing: Fort Worth, TX, 1992; pp 100−101.
(23) Altomare, A.; Cascarano, G.; Giacovazzo, C.; Burla, M. C.; Polidori, G.; Camalli, M. *J. Appl. Crystallogr.* **1994**, *27*, 435−442.
(24) Sheldrick, G. M. *SHELXL97, Program for the Refinement of Crystal Structures*; University of Göttingen, Germany.

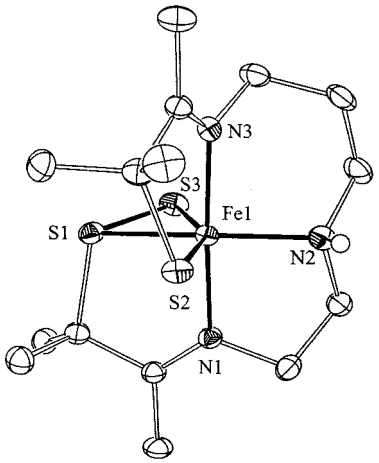

Figure 1. ORTEP diagram of alkyl persulfide ligated [Fe(III)($S_2^{Me2}N_3$-(Et,Pr))-S^{pers}]$^+$ (**2**), showing 50% probability ellipsoids and atom labeling scheme. All H atoms, except for the N(2)−H proton, have been omitted for clarity.

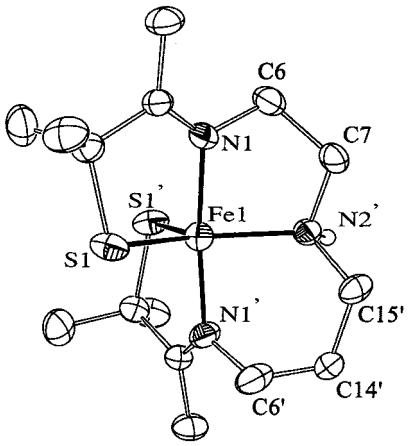

Figure 2. ORTEP diagram of five-coordinate [Fe(III)($S_2^{Me2}N_3$(Et,Pr))]$^+$ (**3**) showing 50% probability ellipsoids and atom labeling scheme. All H atoms, except for the N2′−H proton, have been omitted for clarity.

Results and Discussion

Influence of Amine Ligand on the Product of Metal-Templated Synthesis. As shown previously by our group,[12] condensation of *N*-(3-aminopropyl)-1,3-propanediamine (Pr,Pr-amine) with 2 equiv of 3-methyl-3-mercaptobutanone on an Fe^{2+} template, followed by oxidation with ferrocenium, affords five-coordinate [Fe(III)($S_2^{Me2}N_3$(Pr,Pr))]PF_6 (**1**) (Scheme 1a). When *N*-(2-aminoethyl)-1,3-propanediamine (Et,Pr-amine) is used in place of the Pr,Pr-amine, a six-coordinate η^2-alkyl persulfide ligated complex, [Fe(III)($S_2^{Me2}N_3$(Et,Pr))-S^{pers}]PF_6 (**2**), is obtained (Scheme 1b), instead of the expected five-coordinate analogue of **1**. Persulfide-ligated **2** is the only isolable product in this reaction. Its synthesis is highly reproducible, and yields are always less than 50%. The Fe(II) precursor to **2**, [$Fe^{II}S_2^{Me2}N_3$(Et,Pr)], is five-coordinate, and lacking the extra alkyl persulfide sulfur, and can be isolated as a crystalline product prior to oxidation with ferrocenium. This reduced compound is extremely air sensitive, making further characterization impossible. Oxidized **2** is irreversibly reduced ($E_p = -790$ mV vs SCE), suggesting that an irreversible reaction, possibly desulfurization, occurs following its reduction.

Although there are numerous examples of transition-metal compounds containing an η^2-coordinated disulfido (S_2^{2-}) ligand,[25−32] there are only a small number known to contain an η^2-coordinated alkyl persulfide (R−S_2^-) ligand.[33−35] Most of these were prepared via the alkylation of a disulfido ligand.[34,36−39] Of the known η^2-alkyl persulfide complexes, only three, containing either a second (Mo) or third (W, Os) row transition metal, were stable enough to be crystallographically characterized.[35,36,40] Complex **2** represents the first structurally characterized example of a first-row transition-metal η^2-alkyl persulfide complex.

Structure of Persulfide-Ligated [Fe(III)($S_2^{Me2}N_3$(Et,Pr))-S^{pers}]PF_6 (2). Single crystals of oxidized **2** were obtained via the slow diffusion of Et_2O into an MeCN solution at ambient temperature. As shown in the ORTEP diagram of Figure 1, the Fe(III) ion of **2** sits in a highly distorted octahedral environment. Angles in the FeS_3N2 plane vary from 51.85(3)° to 108.25(9)° (Table 2). The iron−thiolate distance Fe−S2 (2.169(1) Å) is rather short for a low-spin, six-coordinate Fe(III) complex.[12,41−47] The iron−persulfide distances are also unusual in that the bond to the anionic sulfur (Fe−S3 = 2.369(1) Å) is longer, as opposed to shorter, than the bond to the neutral sulfur Fe−S1 = 2.221(1) Å). With side-on alkyl peroxide complexes (e.g., Ti(η^2-O−O^t-Bu))[60] the opposite is true; i.e., the bond to the terminal

(25) Yuki, M.; Kuge, K.; Okazaki, M.; Mitsui, T.; Inomata, S.; Tobita, H.; Ogino, H. *Inorg. Chim. Acta* **1999**, *291*, 395−402.
(26) Lopez, L. L.; Gabay, J.; Haltiwanger, R. C.; Green, K.; Allshouse, J.; Casewit, C.; Rakowski DuBois, M. *Organometallics* **1993**, *12*, 4764−4770.
(27) Houser, E. J.; Dev, S.; Ogilvy, A. E.; Rauchfuss, T. B.; Wilson, S. R. *Organometallics* **1993**, *12*, 4678−4681.
(28) Sweeney, Z. K.; Polse, J. L.; Andersen, R. A.; Bergman, R. G.; Kubinec, M. G. *J. Am. Chem. Soc.* **1997**, *119*, 4543−4544.
(29) McConnachie, C. A.; Stiefel, E. I. *Inorg. Chem.* **1999**, *38*, 964−972.
(30) Hagadorn, J. R.; Arnold, J. *Organometallics* **1998**, *17*, 1355−1368.
(31) Shen, J.; Stevens, E. D.; Nolan, S. P. *Organometallics* **1998**, *17*, 3875−3882.
(32) Brunner, H. W., J.; Gehart, G.; Leblanc, J.-C.; Moïse, C. *Organometallics* **1996**, *15*, 1327−1330.
(33) Legzdins, P.; Sánchez, L. *J. Am. Chem. Soc.* **1985**, *107*, 5525−5526.
(34) Floriani, C.; Gambarotta, S.; Chiesi-Villa, A.; Guastini, C. *J. Chem. Soc., Dalton Trans.* **1987**, 2099−2103.
(35) Song, L.-C.; Hu, Q.-M.; Qin, X.-D. *J. Chem. Res., Synop.* **1999**, 84−85.
(36) Clark, G. R.; Russell, D. R. *J. Organomet. Chem.* **1979**, *173*, 377−387.
(37) Leonard, K.; Plute, K.; Haltiwanger, R. C.; Rakowski DuBois, M. *Inorg. Chem.* **1979**, *18*, 3246−3251.
(38) Goh, L. Y.; Hambley, T. W.; Robertson, G. B. *Organometallics* **1987**, *6*, 1051−1057.
(39) Leblanc, J.-C.; Moise, C.; Volpato, F.; Brunner, H.; Gehart, G.; Wachter, J.; Nuber, B. *J. Organomet. Chem.* **1995**, *485*, 237−242.
(40) Evans, S. V.; Legzdins, P.; Rettig, S. J.; Sánchez, L.; Trotter, J. *Organometallics* **1987**, *6*, 7−9.
(41) Fallon, G. D.; Gatehouse, B. M. *J. Chem. Soc., Dalton Trans.* **1975**, 1344−1347.
(42) Shoner, S. C.; Barnhart, D.; Kovacs, J. A. *Inorg. Chem.* **1995**, *34*, 4517−4518.
(43) Nivorozhkin, A. L.; Uraev, A. I.; Bondarenko, G. I.; Antsyshkina, A. S.; Kurbatov, V. P.; Garnovskii, A. D.; Turta, C. I.; Brashoveanu, N. D. *Chem. Commun.* **1997**, 1711−1712.
(44) Koch, W. O.; Schünemann, V.; Gerdan, M.; Trautwein, A. X.; Krüger, H.-J. *Chem. Eur. J.* **1998**, *4*, 686−691.
(45) Noveron, J. C.; Olmstead, M. M.; Mascharak, P. K. *Inorg. Chem.* **1998**, *37*, 1138−1139.
(46) Noveron, J. C.; Herradora, R.; Olmstead, M. M.; Mascharak, P. K. *Inorg. Chim. Acta* **1999**, *285*, 269−276.
(47) Jackson, H. L.; Shoner, S. L.; Cowen, J. A.; Lovell, S.; Barnhart, D.; Kovacs, J. A. *Inorg. Chem.* **2001**, *40*, 1646−1653.

Table 1. Crystallographic Data for $[Fe^{III}(S_2^{Me2}N_3(Et,Pr))\text{-}S^{pers}]PF_6$ (**2**), $[Fe^{III}(S_2^{Me2}N_3(Et,Pr)]PF_6$ (**3**), $[Fe^{III}(S_2^{Me2}N_3(Et,Pr)(N_3)]$ (**3-N_3**), and $[Fe^{II}S_2^{Me2}N_3(Et,Pr)]$

	$[Fe^{III}(S_2^{Me2}N_3(Et,Pr))\text{-}S^{pers}]PF_6$ (**2**)	$[Fe^{III}(S_2^{Me2}N_3(Et,Pr)]PF_6$ (**3**)	$[Fe^{III}(S_2^{Me2}N_3(Et,Pr)(N_3)]$ (**3-N_3**)	$[Fe^{II}S_2^{Me2}N_3(Et,Pr)]\cdot MeCN$
formula	$C_{15}H_{29}F_6FeN_3PS_3$	$C_{15}H_{29}F_6FeN_3PS_2$	$C_{15}H_{29}FeN_6S_2$	$C_{17}H_{32}FeN_4S_2$
fw	548.41	516.35	413.41	412.44
crystal syst	monoclinic	orthorhombic	orthorhombic	monoclinic
space group	*Cc* (No. 9)	*Pccn* (No. 56)	*Pbca* (No. 61)	$P2_1/c$ (No. 14)
Z	4	4	8	4
a (Å)	17.9869(6)	8.8920(4)	11.0237(2)	9.652(2)
b (Å)	11.8622(2)	13.4838(3)	11.5374(3)	19.301(4)
c (Å)	11.3417(4)	18.3463(8)	30.8031(7)	11.789(2)
α (deg)	90	90	90	90
β (deg)	110.4440(13)	90	90	104.51(3)
γ (deg)	90	90	90	90
V (Å^3)	2267.49(12)	2199.68(15)	3917.69(15)	2126.2(7)
T (K)	161(2)	161(2)	161(2)	183(2)
$R_1{}^a$ ($wR_2{}^b$)	0.0391 (0.1051)	0.0444 (0.1268)	0.0427 (0.1086)	0.0471 (0.1521)

^{a} $R_1 = \sum||F_o| - |F_c||/\sum|F_o|$. ^{b} $wR_2 = \{\sum[w(F_o^2 - F_c^2)^2]/\sum[w(F_o^2)^2]\}^{1/2}$.

Scheme 1

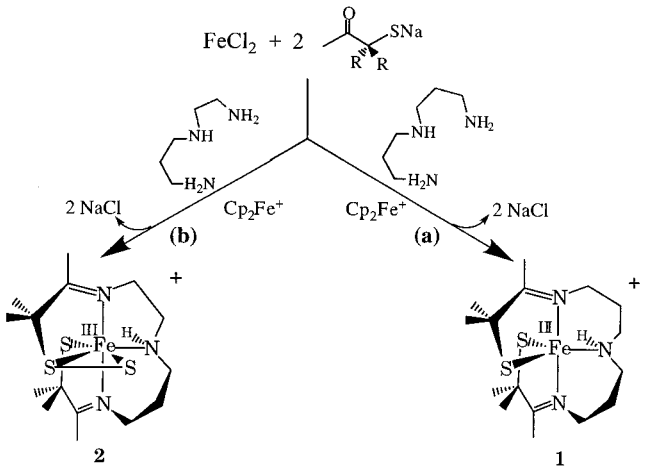

Scheme 2

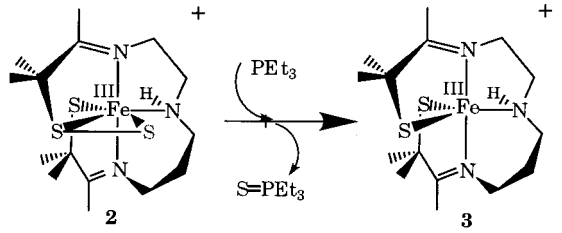

anionic oxygen is the shorter of the two M−O bonds. The persulfide S1−S3 distance (2.011(1) Å), on the other hand, does not differ from previously reported transition-metal η^2-alkyl persulfide structures (mean = 2.02(1) Å).[35,36,40] This distance is, however, slightly shorter than the average S−S distance (2.05(1) Å) in α-S_8.[48]

Synthesis of Five-Coordinate $[Fe(III)(S_2^{Me2}N_3(Et,Pr))]PF_6$ (3) via Sulfur-Atom Extraction from 2. The persulfide sulfur in **2** (S3) can be abstracted using PEt_3 to afford five-coordinate $[Fe(III)(S_2^{Me2}N_3(Et,Pr))]PF_6$ (**3**; Scheme 2). The other product of this reaction was shown to be triethylphosphine sulfide by mass spectrometry and ^{31}P NMR.

(Et,Pr)-ligated **3** is an analogue of (Pr,Pr)-ligated $[Fe(III)(S_2^{Me2}N_3(Pr,Pr))]PF_6$ (**1**), but contains one fewer methylene in its ligand backbone. (Et,Pr)-ligated **3** is reduced at a potential of −455 mV (vs SCE)) in MeOH—a potential which is comparable to that ($E_{1/2}$ = −400 mV (vs SCE)) of (Pr,Pr)-ligated **1**.

Influence of Ligand Constraints on the Structural and Magnetic Properties of Five-Coordinate $[Fe(III)(S_2^{Me2}N_3(Et,Pr))]PF_6$ (3). Single crystals of $[Fe(III)(S_2^{Me2}N_3(Et,Pr))]PF_6$ (**3**) were obtained via layered diffusion of Et_2O into a CH_2Cl_2 solution. Cationic **3** (Figure 2) was located on a crystallographic 2-fold axis which bisects the S1−Fe−S1′ angle. Amine nitrogen N2 was found to lie 0.51 Å away from this 2-fold axis, and as a result, N2 and the ethyl and propyl carbons (C7, C14, C15) were found to be disordered, with a 50% occupancy factor. One of the symmetry-equivalent molecules contains the ligand backbone C6−C7−N2′−C15′−C14′−C6′, while the other contains C6−C14−C15−N2−C7′−C6′ (Figures S-8 and S-9). This disorder is confined to the asymmetrical region of the ligand backbone, however, so that most of the molecule remains unaffected; four out of five of the coordinated atoms are *not* disordered. Atoms C1−C6, N1, and S2 were given site occupancies of 1.0. As shown in the ORTEP diagram of Figure 2, the Fe(III) ion of (Et,Pr)-ligated **3** is contained in a highly distorted geometry, which lies approximately halfway between trigonal bipyramidal and square pyramidal. Comparison of the *τ*-values[49] for (Et,Pr)-ligated **3** ($\tau = 0.539$)[50] vs (Pr,Pr)-ligated **1** ($\tau = 0.763$) shows *that removal of a methylene unit* from the ligand backbone of **1** *causes the structure to distort dramatically* toward a more square pyramidal structure. This distortion results in a more open S(1)−Fe−N(2) angle in **3** (141.8(1)°) vs **1** (132.3(1)°; Table 2; Figure 3).

In Table 2, bond distances and angles in five-coordinate $[Fe(III)(S_2^{Me2}N_3(Et,Pr))]PF_6$ (**3**) are compared with its reduced derivative $[Fe(II)(S_2^{Me2}N_3(Et,Pr))]$, its alkyl persulfide ligated precursor $[Fe(III)(S_2^{Me2}N_3(Et,Pr))\text{-}S^{pers}]PF_6$ (**2**), and its (Pr,Pr) analogue $[Fe(III)(S_2^{Me2}N_3(Pr,Pr))]PF_6$ (**1**). As one would expect, metal−ligand bond distances are noticeably

(48) Rettig, S. J.; Trotter, J. *Acta Crystallogr., Sect. C* **1987**, *C43*, 2260−2262.

(49) Addison, A. W.; Rao, T. N.; Reedijk, J.; van Rijn, J.; Verschoor, G. C. *J. Chem. Soc., Dalton Trans.* **1984**, 1349−1356.

(50) The parameter τ is defined as the difference between the largest (*a*) and second largest (*b*) angles divided by 60° ($(a - b)/60° = \tau$), where $\tau = 1$ for ideal trigonal bipyramidal geometry vs $\tau = 0$ for ideal square pyramidal geometry.

Table 2. Selected Bond Lengths (Å) and Angles (deg) for [Fe(III)($S_2^{Me2}N_3$(Pr,Pr))]PF_6 (**1**),[a] [Fe(III)$S_2^{Me2}N_3$(Pr,Pr)(N_3))] (**1-N_3**),[a] [Fe(III)$S_2^{Me2}N_3$(Et,Pr))-S^{pers}]PF_6 (**2**), [Fe(III)($S_2^{Me2}N_3$(Et,Pr))]PF_6 (**3**),[b] [Fe(III)($S_2^{Me2}N_3$(Et,Pr))(N_3)] (**3-N_3**), and [Fe(II)$S_2^{Me2}N_3$(Et,Pr))]·MeCN

	1	**1-N_3**	**2**	**3**[b]	**3-N_3**	[$Fe^{II}S_2^{Me2}N_3$ (Et,Pr)]
Fe−S1	2.133(2)	2.196(1)	2.2209(9)	2.117(1)	2.2226(7)	2.342(1)
Fe−S2	2.161(2)	2.209(1)	2.1694(8)	2.117(1)[b]	2.1994(6)	2.317(1)
Fe−S3	N/A	N/A	2.3687(9)	N/A	N/A	N/A
S1−S3	N/A	N/A	2.011(1)	N/A	N/A	N/A
Fe−N1	1.967(4)	1.978(3)	1.944(2)	1.924(2)	1.916(2)	2.123(4)
Fe−N2	2.049(4)	2.157(3)	1.993(3)	2.010(4)	2.061(2)	2.216(4)
Fe−N3	1.954(4)	1.970(3)	1.971(2)	1.924(2)[b]	1.963(2)	2.116(4)
Fe−N4	N/A	2.061(4)	N/A	N/A	2.093(2)	N/A
N1−Fe−N2	94.2(2)	99.7(1)	85.2(1)	86.4(1)[b]	86.28(7)	77.0(1)
N1−Fe−N3	178.1(2)	174.9(1)	175.6(1)	174.1(1)[b]	173.20(8)	157.8(1)
N1−Fe−S1	86.7(1)	84.8(1)	84.99(8)	86.68(7)	86.57(6)	81.6(1)
N2−Fe−N3	86.2(2)	82.2(1)	92.1(1)	87.9(1)[b]	88.69(7)	81.0(1)
N2−Fe−S1	132.3(1)	172.5(1)	149.86(9)	141.8(1)[b]	167.85(5)	123.0(1)
N2−Fe−S2	106.5(1)	90.6(1)	108.25(9)	112.5(1)[b]	93.25(5)	114.0(1)
N2−Fe−S3	N/A	N/A	99.23(9)	N/A	N/A	N/A
N3−Fe−S2	86.4(1)	84.4(1)	85.13(8)	86.68(7)[b]	84.74(6)	83.1(1)
N3−Fe−S3	N/A	N/A	96.80(8)	N/A	N/A	N/A
S1−Fe−S2	121.0(1)	95.3(1)	100.57(3)	105.67(5)[b]	96.68(3)	122.84(5)
S1−Fe−S3	N/A	N/A	51.85(3)	N/A	N/A	N/A
S2−Fe−S3	N/A	N/A	152.38(4)	N/A	N/A	N/A
τ	0.763	N/A	N/A	0.539	N/A	0.580

[a] Ellison, J. J.; Nienstedt, A.; Shoner, S. C.; Barnhart, D.; Cowen, J. A.; Kovacs, J. A. *J. Am. Chem. Soc.* **1998**, *120*, 5691−5700. [b] S1′, N1′, and N2 in **3** correspond to S2, N3, and N2 in the other compounds.

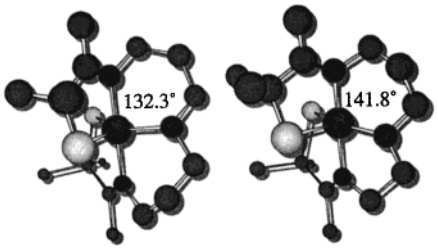

Figure 3. Chem 3D figure comparing the structures of [Fe(III)($S_2^{Me2}N_3$-(Pr,Pr))]$^+$ (**1**) and [Fe(III)($S_2^{Me2}N_3$(Et,Pr))]$^+$ (**3**). The more open binding site is indicated.

shorter in oxidized **3** relative to [Fe(II)($S_2^{Me2}N_3$(Et,Pr)]. Removal of the persulfide sulfur from **2** also causes the bond distances to decrease, but less substantially than with oxidation (Table 2). This reflects the expected differences between six- and five-coordinate structures. Removal of a methylene unit from the ligand backbone of **1** also causes the metal−ligand bond distances to decrease (Table 2). For example, the mean Fe−S and Fe−N_{imine} distances shorten by 0.03(2) and 0.04(1) Å, respectively, and the Fe−N_{amine} bond distance shortens by 0.04(1) Å in **3** vs **1**. This structural change, although not anticipated, can be attributed to differences in spin states.

Removal of a methylene unit from the ligand backbone of five-coordinate [Fe(III)($S_2^{Me2}N_3$(Pr,Pr))]PF_6 (**1**) has a noticeable effect on its magnetic properties. (Et,Pr)-ligated **3** is $S = 1/2$ over a wide temperature range, whereas **1** exists as a mixture of spin states at ambient temperature. This is illustrated in Figure 4, which shows the 2−300 K temperature dependence of the inverse susceptibility, χ^{-1}, of (Pr,Pr)-ligated **1** vs (Et,Pr)-ligated **3**. At low temperatures (Pr,Pr)-ligated **1** follows the Curie law, with a μ_{eff} consistent with a low-spin $S = 1/2$ ground state. However, at temperatures above 100 K an increase in the effective moment of **1** is observed due to the thermal population of a higher spin state.[12] Higher spin states are partially occupied at the

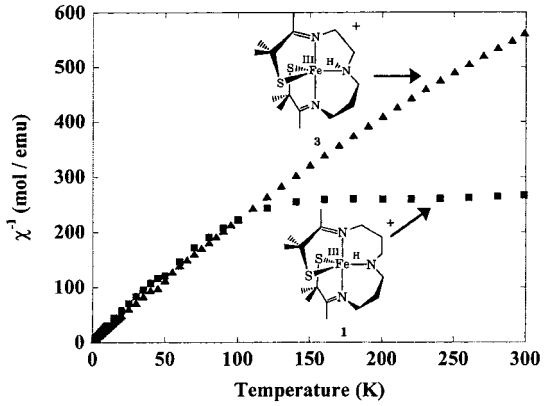

Figure 4. Temperature dependence of reciprocal molar susceptibilities, χ^{-1}, for [Fe(III)($S_2^{Me2}N_3$(Pr,Pr))]PF_6 (**1**) (squares) and [Fe(III)($S_2^{Me2}N_3$(Et,-Pr))]PF_6 (**3**) (triangles).

temperature (183 K) of the X-ray structure determination. This χ^{-1} vs T data can be fitted to an $S = 1/2 \rightarrow S = 3/2$ equilibrium, with a 300 cm^{-1} separation between states. A Boltzmann distribution analysis of this equilibrium indicates that ∼32% of **1** is $S = 3/2$ at ambient temperature. In contrast, (Et,Pr)-ligated **3** is 100% $S = 1/2$ at ambient temperature. As shown in Figure 4, complex **3** follows the Curie law ($\chi \propto 1/T$) over the entire temperature range examined (2−300 K), including the temperature at which the X-ray structure was determined. These differences in ambient temperature magnetic properties would be expected to influence reactivity (vide infra). The ground spin state assignment of **3** is supported by the low temperature EPR spectrum shown in Figure 5. At 130 K both **1** and **3** are characterized by pseudorhombic $S = 1/2$ EPR signals with g-values of 2.14, 2.07, and 2.01 (**1**)[51] and 2.12, 2.07, and

(51) EPR spectra previously reported (ref 12) were measured in a MeOH/EtOH glass. Recent data, however, suggest that **3** binds MeOH at low temperatures. To measure five-coordinate **1** and **3**, spectra were measured in a noncoordinating solvent system, i.e., CH_2Cl_2/toluene.

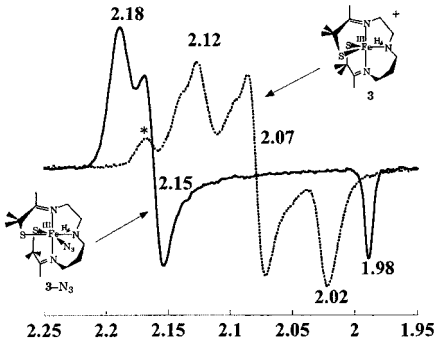

Figure 5. X-Band EPR spectra of **3** and **3-N$_3$** in CH_2Cl_2/toluene (1:1) glass at 130 K. * = acetonitrile-ligated impurity (**3-MeCN**).[57]

Scheme 3

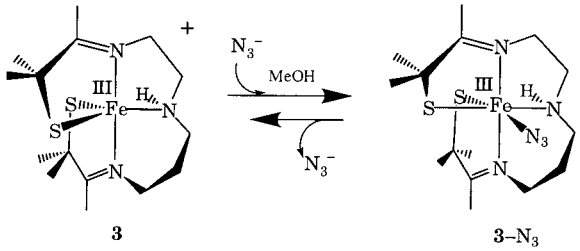

2.02 (**3**), respectively. No signals attributable to high- or intermediate-spin species were detected for **1** at this temperature. At the higher temperatures required to populate the $S = 3/2$ spin state, no EPR signal is detectable, due to rapid relaxation.

Influence of Structure on the Reactivity Properties of Five-Coordinate [Fe(III)($S_2^{Me2}N_3$(Et,Pr))]PF_6 (3) vs [Fe(III)($S_2^{Me2}N_3$(Pr,Pr))]PF_6 (1). One of the most significant structural differences between (Pr,Pr)-ligated **1** and (Et,Pr)-ligated **3** is that an angle in the equatorial plane (S1−Fe−N2) opens from 132.3(1)° (in **1**) to 141.8(1)° (in **3**) (Figure 3). Azide and NO have been shown to bind to this open angle of **1**.[12,13] Similarly, azide will bind to the more open site of **3** (Scheme 3). This reaction is irreversible in CH_2Cl_2, THF, and MeCN. However, in MeOH this reaction is reversible (Scheme 3), and low temperatures are required to generate substantial quantities of **3-N$_3$**. The reversibility of this reaction was demonstrated by examining the variable temperature electronic absorption spectrum (Figure 6). Azide coordination causes the bands near 500 nm, associated with five-coordinate **3**, to disappear, and two new bands at 760 and 470 nm to grow in. The band near 700 nm is characteristic of six-coordinate, low-spin, *cis*-dithiolate ligated Fe(III),[12,41,42,45] and has been assigned as a sulfur-to-metal charge transfer (LMCT) transition.[61] When this reaction is monitored by EPR in CH_2Cl_2/toluene glass, azide causes the signal associated with **3** to open up to a more near-axial pattern with *g*-values of 2.18, 2.15, and 1.98 (Figure 5). These *g*-values are comparable to those of azide-ligated **1** (**1-N$_3$**) at 2.23, 2.15, and 1.98.

Previous studies had shown that azide binds reversibly to (Pr,Pr)-ligated **1** in MeOH, to a site which is trans to a thiolate sulfur, with a ΔH of -5.2 ± 0.5 kcal mol^{-1} and a ΔS of -12.4 ± 2.2 eu.[12] To quantitatively determine how the more distorted structure of **3**, with its more open S1−

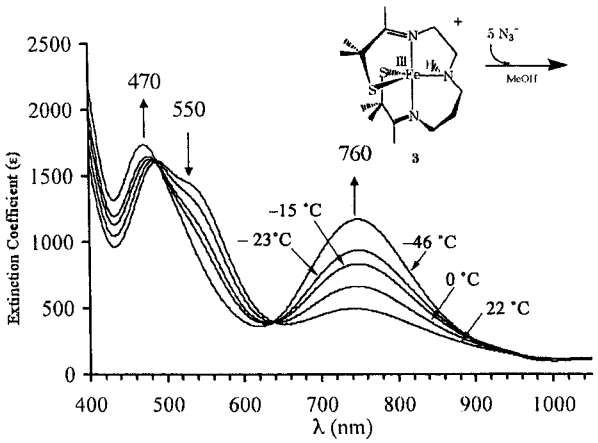

Figure 6. Temperature-dependent electronic absorption spectrum of [Fe(III)($S_2^{Me2}N_3$(Et,Pr))]PF_6 (**3**) + N_3^- (5 mM) in MeOH ([**3**]$_0$ = 1 mM, I = 0.06 mol/L). As the temperature is lowered, two bands corresponding to [Fe(III)($S_2^{Me2}N_3$(Et,Pr))(N_3)]PF_6 (**3-N$_3$**) grow in at 760 and 470 nm, and a shoulder at 550 nm, corresponding to **3**, disappears. The ratio of azide-bound to five-coordinate **3** changes from 34% at 22 °C, to 49% at 0 °C, 67% at −15 °C, 75% at −23 °C, and 95% at −46 °C.

Table 3. Equilibrium Constants for the Reaction of [Fe^{III}($S_2^{Me2}N_3$(Et,Pr)]PF_6 (**3**) with Azide in MeOH to Form [Fe^{III}($S_2^{Me2}N_3$(Et,Pr)(N_3)] (**3-N$_3$**)

T (°C)	K_{eq} (M^{-1})
22	110 ± 20
0	210 ± 40
−15	470 ± 90
−23	720 ± 140
−46	4950 ± 800

Fe−N2 angle, influences its reactivity toward "substrates", the thermodynamics of azide binding to **3** (Scheme 3) were also examined. Thermodynamic measurements were performed according to Drago[52,53] under the same conditions ([I] = 0.06 M in methanol) used to measure equilibrium constants for azide binding to (Pr,Pr)-ligated **1**.[12] Equilibrium constants (K_{eq}) were determined at five different temperatures (Table 3; Figure 6), and a van't Hoff plot was used to interpret the data. It was determined that the reaction shown in Scheme 3 occurs with a $\Delta H = -7.5 \pm 0.6$ kcal mol^{-1} and a $\Delta S = -16.6 \pm 2.5$ eu. That the entropies of azide binding to **1** and **3** are nearly identical is not surprising, given that azide binding occurs through identical associative pathways for both **1** and **3**.[54] The ΔH associated with azide binding to (Et,Pr)-**3**, on the other hand, is significantly more negative than that of (Pr,Pr)-ligated **1**: *an additional 2.3 kcal mol^{-1} energy is released when azide binds to* **3** *vs* **1**. This translates into a nearly 10-fold increase in K_{eq} at any given temperature. This increase in ΔH could be a consequence of a decrease in the stability of **3** relative to **1**, an increase in the stability of **3-N$_3$** relative to **1-N$_3$**, or some combination of both. To gain insight regarding the relative energies of azide-ligated **1-N$_3$** vs **3-N$_3$**, and five-coordinate **1** vs **3**, and to examine the barriers to azide binding to **1** vs **3**, kinetic studies were performed.

(52) Epley, T. D.; Drago, R. S. *J. Am. Chem. Soc.* **1969**, *91*.
(53) Guidry, R. M.; Drago, R. S. *J. Am. Chem. Soc.* **1973**, *95*, 6645.
(54) Rates are first order in azide and first order in iron compound for both **3** and **1** in MeOH, indicating that these reactions occur via an associative mechanism.

The rates for azide binding to **1** and **3** were determined under pseudo-first-order conditions at ambient temperature, using a stopped-flow instrument. In MeOH, rate constants for the reaction of **1** and **3** with azide were found to be nearly identical: $k_{on} = 1.1$ (± 0.6) and 1.9 (± 0.6) M^{-1} s^{-1} for **3** and **1**, respectively. From the ambient temperature K_{eq} and k_{on} values, it was then possible to determine the rate constants for azide dissociation (k_d) from **1** and **3**. Azide dissociation from **1-N$_3$** occurs an order of magnitude faster than it does from **3-N$_3$**, with $k_d = 1.4$ (± 0.5) $\times 10^{-1}$ (for **1-N$_3$**) and 1.0 (± 0.5) $\times 10^{-2}$ s^{-1} (for **3-N$_3$**). These rate constants are both much larger than one would expect for low-spin Fe^{III}. This is not the case when, for example, azide is bound trans to a nitrogen as opposed to a sulfur. As an example, the low-spin complex $[Fe^{III}(S^{Me2}N_4(tren))(azide)]^+$,[55] which contains azide bound trans to a nitrogen, displays no equilibrium toward the azide-free complex in MeOH, indicating that k_d is extremely small.[56] This suggests that the trans thiolate increases the reactivity of both **3-N$_3$** and **1-N$_3$** by labilizing the azide. In fact, we recently described[59] the kinetics of ligand dissociation from the low-spin ($S = 0$) Co^{III} analogue of **1-N$_3$**, and demonstrated that the thiolate which is trans to the azide causes the rate of ligand dissociation to increase 4 orders of magnitude relative to substitution-inert (low-spin) $Co^{III}(H_2O)(NH_3)_5^{3+}$. In this study, the relative rates of azide dissociation seem to indicate that the difference in equilibrium constants for azide binding to **1** and **3** in MeOH results from an increased stability of **3-N$_3$** vs **1-N$_3$**. However, since MeOH can effectively solvate azide, it is possible that these data (i.e., k_{on}, and thus k_d, since k_d is calculated from K_{eq} and k_{on}) predominantly reflect the desolvation of the coordinating azide anion, as opposed to an inherent increase in the stability of **3-N$_3$** vs **1-N$_3$**. Kinetics of reactions involving **3** in MeOH are also complicated by the fact that MeOH coordinates to **3**, although this only occurs to a significant extent at temperatures below -20 °C.[57] Complex **1**, on the other hand, does not bind MeOH at temperatures above -173 °C.

To determine the extent to which solvation of azide by MeOH, and possibly coordination of MeOH to **3**, affects the rates of azide binding to **1** and **3**, kinetic measurements were performed in both a polar aprotic (MeCN) and a noncoordinating aprotic (CH_2Cl_2) solvent. In acetonitrile, the rate of azide binding to **3** was significantly increased relative to that in methanol, with $k_{on} = 5.9 \pm 0.3$ M^{-1} s^{-1}. In methylene chloride, the rate of azide binding to **3** was even faster, with $k_{on} = 9.3 \pm 0.3$ M^{-1} s^{-1}. The rates of azide binding to (Pr,Pr)-ligated **1**, on the other hand, were essentially solvent independent (Table 4). The increased k_{on} for azide binding to **3** in methylene chloride vs acetonitrile could be a result of coordination of acetonitrile to the metal center of **3**.[57] The incoming azide would have to displace a loosely bound acetonitrile from **3**, and this would be expected to decrease the rate of azide binding in this solvent. In fact, it has been shown spectrophotometrically that this is the case.[57] In contrast, MeCN has never been shown to coordinate to **1** at ambient temperature; therefore, azide would not have to displace MeCN from the open coordination site of **1**, thus explaining why the rates of azide binding to **1** are nearly identical in CH_2Cl_2 and MeCN. MeOH was also found to bind to **3** (and not to **1**) at low temperatures;[57] however, the K_{eq} for MeOH binding was found to be an order of magnitude smaller than K_{eq} for MeCN binding (1.6(3) M^{-1} at -70 °C), indicating that MeOH competes less effectively for this open coordination site than MeCN. This would suggest that the slower on rates in MeOH are mainly due to solvation of azide, as opposed to competition for the open site. The fact that on rates are identical for **3** and **1** in MeOH supports this. Since CH_2Cl_2 would not be expected to coordinate to **3** or to solvate azide, the k_{on} value in this solvent may be the closest to representing the coordination of naked azide to bare five-coordinate **3**.

Table 4. Rate Constants for Azide Binding to $[Fe(III)(S_2Me2N_3(Et,Pr))]^+$ (**3**) vs $[Fe(III)(S_2Me2N_3(Pr,Pr))]^+$ (**1**)

	3 + N_3	**1** + N_3
k_{on}(CH_2Cl_2, 22 °C)	9.3(3) M^{-1} s^{-1}	2.5(5) M^{-1} s^{-1}
k_{on}(MeCN, 22 °C)	5.9(3) M^{-1} s^{-1}	2.2(6) M^{-1} s^{-1}
k_{on}(MeOH, 22 °C)	1.1(6) M^{-1} s^{-1}	1.9(6) M^{-1} s^{-1}
k_{off}(MeOH, 22 °C)	1.0(5) $\times 10^{-2}$ s^{-1}	1.4(5) $\times 10^{-1}$ s^{-1}

The results of these kinetic studies are summarized in Table 4.[58] Most notable is that *there is a substantial difference in k_{on} values for azide binding to* **1** *vs* **3** *when the effects of a polar protic solvent (MeOH) are negated: rates are faster for azide binding to* **3** *relative to* **1**. This is a consequence of either the more open S1−Fe−N2′ angle (the binding site) of **3** relative to **1** or differences in the LUMO (vs SOMO) orbital population (i.e., spin-state differences): with **3** azide approaches an orbital ($d_{x^2-y^2}$) that is empty, whereas with **1** this orbital is half-filled (30% of the time, since 30% of the sample is $S = 3/2$ at ambient temperature). Also, given that the reaction mechanisms for azide binding to **1** and **3** are identical,[54] less structural rearrangement would be required to convert five-coordinate **3** to six-coordinate **3-N$_3$**. With **3**, its S1−Fe−N2 angle (141.8(1)° vs 132.3(1)° in **3** and **l**, respectively) starts out closer to the near-linear value of the product (167.85(5)° in **3-N$_3$** (below); 172.5(1)° in **1-N$_3$**).

To determine quantitatively the amount of structural rearrangement that is required for azide to bind to **3**, an X-ray crystal structure of **3-N$_3$** was performed. Bond lengths and angles of azide-ligated **1-N$_3$** vs **3-N$_3$** were also compared to determine if there was any structural evidence for inherent differences in stability. Single crystals of **3-N$_3$** were isolated by layering Et_2O onto a cooled (-35 °C) THF solution. As

(55) Shearer, J.; Nehring, J.; Kaminsky, W.; Kovacs, J. A *Inorg. Chem.* **2001**, *40*, 5483−5484.
(56) Shearer, J.; Kaminsky, W.; Scarrow, R. C.; Kovacs, J. A. *Inorg. Chem.*, submitted for publication.
(57) Shearer, J.; Jackson, H. L.; Schweitzer, D.; Rittenberg, D.; Leary, T. M.; Kaminsky, W.; Scarrow, R. C.; Kovacs, J. A. *J. Am. Chem. Soc.*, in press.
(58) Both **1** and **3** appear to quantitatively bind azide in both CH_2Cl_2 and MeCN at ambient temperature, so k_d could not be determined in a manner similar to that used for MeOH
(59) Shearer, J.; Kung, I. Y.; Lovell, S.; Kaminsky, W.; Kovacs, J. A. *J. Am. Chem. Soc.* **2001**, *123*, 463−468.
(60) Boche, G.; Mobus, K.; Harms, K.; Marsch, M. *J. Am. Chem. Soc.* **1996**, *118*, 2770−2771.
(61) Kennepohl, P.; Schweitzer, D.; Jackson, H. L.; Kovacs, J. A.; Solomon, E. I., manuscript in preparation.

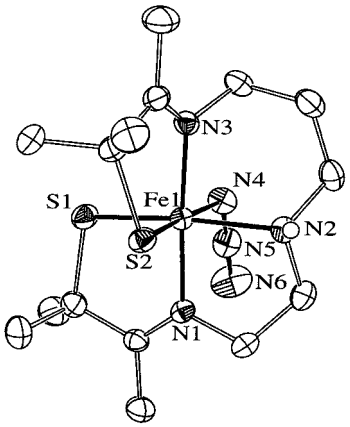

Figure 7. ORTEP diagram of [Fe(III)($S_2^{Me2}N_3$(Et,Pr))(N_3)] (**3-N_3**) showing 50% probability ellipsoids and atom labeling scheme. All H atoms, except for the N(2)−H proton, have been omitted for clarity.

illustrated in the ORTEP diagram of **3-N_3** in Figure 7, azide binds trans to a thiolate sulfur (S2), which is similar to its mode of binding (i.e., trans to a thiolate) to (Pr,Pr)-ligated **1**. Comparison of the metrical parameters for five-coordinate **3** and azide-bound **3-N_3** (Table 2) shows that the angle into which the azide is inserted (S1−Fe−N2) opens from 141.8-(1)° (in **3**) to 167.85(5)° (in **3-N_3**). These structural changes are more pronounced when azide binds to **1**: with **1** the angle into which the azide is inserted opens by 40.2° [12] (Table 2). This supports the notion that structural distortion in **3** increases its substrate binding rates by decreasing the requisite structural rearrangement. As shown in Table 2, the bond distances also lengthen upon azide coordination, just as one would expect upon the conversion of a five-coordinate (**3**) to a six-coordinate (**3-N_3**) compound. Changes to Fe−S1 relative to Fe−S2 indicate that azide does not exert a noticeable trans influence. Azide-bound **3-N_3** and **1-N_3** are structurally very similar. In both, the Fe(III) ion sits in a near-ideal octahedral environment. All angles, with the exception of N1−Fe−N2, are within 6.5° of each other, and bond lengths are nearly identical. This reflects, in part, the virtually identical magnetic properties of **3-N_3** and **1-N_3**. Thus, we have very little structural or physical evidence for significant differences in the relative energies of azide-ligated **3-N_3** vs **1-N_3**.

Conclusions

The work described herein demonstrates how subtle changes to a ligand backbone can dramatically influence the reactivity of a metal ion by distorting its geometry and altering its magnetic properties. Proteins have been shown to enforce unstable geometries (an entatic state) to, for example, enhance electron transfer rates and driving force. This work suggests that the reactivity of a metalloenzyme which is involved in binding substrates can be increased by opening an angle (via, e.g., protein constraints) and thereby (1) making the metal ion more accessible to substrates and (2) decreasing the structural reorganization required to bind substrate. In the model complexes described herein an angle change of ∼10° was shown to increase azide binding rates in CH_2Cl_2 ∼3-fold and to shift the MeOH equilibrium between azide-bound and azide-free (five-coordinate) forms by ∼1 order of magnitude. This subtle angle change, which was induced by removing a single methylene unit from the ligand backbone, was also shown to alter the magnetic properties (i.e., the spin state). Spin-state differences would alter reaction rates by altering the LUMO (vs SOMO) orbital population. Solvent was also shown to have a dramatic influence on azide binding: a change from MeOH to MeCN (or CH_2Cl_2) solvent was shown to convert a reversible reaction to an irreversible one. This illustrates how important the electrostatic and H-bonding character of the active site pocket can be in determining the kinetics and thermodynamics of substrate binding to a metalloenzyme. The (Et,Pr)-ligated Fe(III) complex described herein reacts with a variety of "substrates", including nitriles. These more extensive reactivity studies will be the subject of a future publication.[57]

Acknowledgment. The NIH is gratefully acknowledged for their support (GM45881) of this work. We thank D. Gamelin for extremely helpful discussion regarding the magnetic behavior of **1**, T. Okonogi for assistance with the EPR measurements, H. Jackson for assistance with the CV measurements, and W. Kaminsky for help with the X-ray crystallography.

Supporting Information Available: IR spectra (KBr pellet) of **2**, **3**, and **3-N_3**. UV/vis of **2** and **3** in MeOH. UV/vis of **3-N_3** in CH_2Cl_2. $1/\chi_{M,para}$ versus temperature plots of **2** and **3-N_3**; ORTEP diagram and chemdrawings of **3** showing the disorder about the crystallographically imposed 2-fold axis; X-ray crystallographic files for structures **2**, **3**, **3-N_3**, and [Fe(II)($S_2^{Me2}N_3$(Et,Pr))]. This material is available free of charge via the Internet at http://pubs.acs.org.

IC0109187